 doi:10.20944/preprints201806.0309.v1

Brazing studies of Ti- joint using $Ti_{20}Zr_{20}Cu_{60-x}Ni_x$ (x = 30, 40, and 50) metallic glass ribbon as filler metal

P. Rama Rao*[1, 3], Anil K. Bhatnagar[1], Bhaskar. Majumdar[2] and Sandip Bysakh[3]

[1] School of Engineering Sciences & Technology
University of Hyderabad, Hyderabad 500046, India
[2] Defence Metallurgical Research Laboratory
Kanchanbagh, Hyderabad – 500 058, India
[3]Advanced Mechanical and Material Characterization Division
CSIR-Central Glass and Ceramic Research Institute, Kolkata-700032, India

(*corresponding author: panugothu.ramarao@gmail.com)

Abstract: The present study investigation, our results on characterization of commercially pure-Ti alloy brazed with metallic glass ribbons of $Ti_{20}Zr_{20}Cu_{60-x}Ni_x$ (x = 30, 40, and 50) metallic glass ribbons were produced using a vacuum melt spinner. These ribbons were then used as filler materials for vacuum brazing of two Ti alloy plates at 1268, 1277 and 1279 K for a period of 10 min. Field-Emission Scanning Electron Microscopy (FESEM), Transmission Electron Microscopy (TEM) and the energy dispersive X-ray spectroscopy (EDX). The as-spun ribbons showed fully amorphous structure when examined on both surfaces by XRD and also verified by TEM investigation. The brazing joint of two Ti-plates using the metallic glass ribbon when brazed with Ni_{50} was found to be of very high strength. FESEM characterization of the cross-section of the brazed joints shows sub-micron size grains uniformly distributed in the matrix with brighter appearance. FESEM and EDX analysis revealed that the sub-micron grains are rich in Ti & Ni while the matrix phase mainly consisted of Ti. BSE image along with EDS Analysis indicated that the brazed joint has a presence of $NiTi_2$ and Cu_2 (Ni Zr) phases which could be responsible for increase in the strength of the brazed joint.

Keywords: Metallic glasses, Ti-alloy, Microstructure, Scanning Electron Microscopy and Transmission electron microscopy.

Preprints (www.preprints.org) | NOT PEER-REVIEWED | Posted: 20 June 2018 doi:10.20944/preprints201806.0309.v1

1. Introduction

Brazing is a metal-joining process where a filler metal is heated above its melting point and distribution between two or more closefitting parts [1-4]. This process is considered to be one of the simplest and by far the most widely methods used to join ceramics to metals based on melting, wetting and solidification of a liquid film between the base materials [5,6-10], as reported by Martens et al. (1996). More recently, Sugar et al.(2006) reported that to improve the wetting and adherence of the metal-foil interlayer where the surfaces are in contact during the joining process [11,12], it is essential that the surfaces are prepared (cleanliness) and/or the materials to be joined are conditioned, i.e., an effective metallization (through wetting or flow) is required.

Titanium alloys, due to their high specific strength and good corrosion resistance, are particularly suitable for special applications. CP-Ti (Commercially Pure Titanium), which is unalloyed, ranges in purity from 99.5 to 99.0 wt pct Ti. Titanium exists in two allotropic crystal structures. There area, which has the hexagonal close-packed (HCP) structure, and b, which has the body-centered cubic (BCC) crystal structure. Above the β transus temperature, the hexagonal α-phase is transformed on heating to the BCC β-phase [13-16].The β transus temperature is strongly affected by the alloying elements in CP-Ti, e.g., Fe and interstitial elements, carbon, oxygen, nitrogen, as well as hydrogen.

The scanning, transmission electron microscope (FESEM/TEM), and X-ray diffractometer (XRD) are not satisfactory in analysis of a brazed joint involved with phase transformation. Although FESEM observations present quantitative chemical compositions of the specific phases, it lacks structural data to identify them. For example, the transformation between α and β phases in the titanium alloy could not be accurately identified from FESEM/TEM analyses. On the other hand, the width of a brazed joint is usually below 100 μm, so slicing

Preprints (www.preprints.org) | NOT PEER-REVIEWED | Posted: 20 June 2018 doi:10.20944/preprints201806.0309.v1

different brazed zones in order to make TEM examination is quite difficult. The electron backscatter diffraction (EBSD) technique has made a great achievement in recent years [17, 18]. Therefore, the combination of morphology, element mapping, and crystallographic data makes it possible to analyse such a brazed joint undergoing phase transformation. In this work, the objective of the research is concentrated on the brazing CP-Ti using the $Ti_{20}Zr_{20}Cu_{60-x}Ni_x$ (x = 30, 40, and 50) filler foil. The vacuum brazing has been carried out during the experiment for the sake of comparison. Phase identification, microstructural evolution, and interfacial reaction of the brazed joint are extensively studied in this investigation.

2. EXPERIMENTAL METHODS

The alloy with nominal composition $Ti_{20}Zr_{20}Cu_{60-x}Ni_x$ (x = 30, 40, and 50) is prepared from pure elements (purity > 99.9 wt. %) by arc melting in a titanium-gettered argon atmosphere. For achieving homogeneity in the alloy composition, it is remelted many times. The amorphous ribbon of this compound is prepared using the standard rapid quenching technique. The ribbon is about 25 mm wide and 100 μm thick. The X-ray Diffractometers, used to characterize the sample, is a Bruker machine, Model No. D8. The Field Emission Gun (FEG) is usually a wire of Tungsten (W) Zigma, Carl Zeiss, Germany (FE-SEM, Carl ZEISS, FEG, Ultra 55), 30kV, images were obtained at an operating voltage of 15 kV and the working distance was about 8.5 mm.

Vacuum brazing was performed to braze commercially pure CP-Ti plates using the as spun $Ti_{20}Zr_{20}Cu_{60-x}Ni_x$ (x = 30, 40, and 50) metallic glass ribbon as filler material. The CP-Ti plates measuring 10 mm×7 mm× 3mm were prepared. the lap-butt joint, the CP-Ti plates measuring 5 mm×3 mm×1 mm were first prepared and then steps were cut in EDM using a 0.5 mm wire. Both the brazing ribbons and Ti plates were initially cleaned using acetone and then the ribbons were kept in between the two Ti plates before tightening them using nicrome

Preprints (www.preprints.org) | NOT PEER-REVIEWED | Posted: 20 June 2018 doi:10.20944/preprints201806.0309.v1

wire. The samples were then placed in a vacuum furnace (10^{-3} mbar) and annealed for 10 minutes. The selected temperature for each sample was 20±5°C higher than the solidus temperature of respective ribbon. The samples were then furnace cooled.

3. RESULTS AND DISCUSSION

3.1 Microstructure analysis of Ti/$Ti_{20}Zr_{20}Cu_{30}Ni_{30}$ /Ti composite joint brazed at 1268 K for a period of 10 min

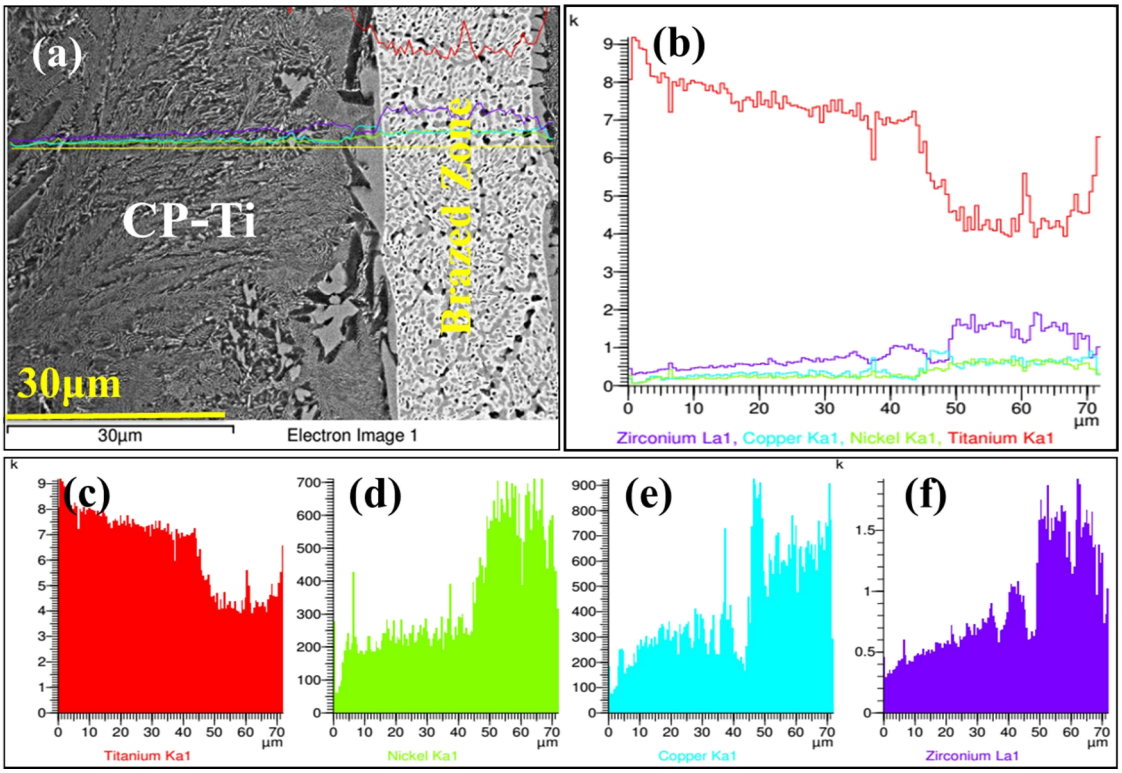

Figure 1. FESEM analysis of Ti/ $Ti_{20}Zr_{20}Cu_{30}Ni_{30}$ /Ti composite joint brazed at 1268 K for a period of 10 min (a) Cross sectional BSE Image (b) corresponding EDS based line scan analysis across 30µm length comprising the CP-Ti pieces on both sides of brazed joint, corresponding concentration profiles of elements :(c)Ti, (d)Ni (e) Cu and (f) Zr.

The FESEM analysis of Ti/$Ti_{20}Zr_{20}Cu_{30}Ni_{30}$/Ti composite joint brazed at 1268 K for a period of 10 min is shown in fig.1. Figure 1(a) shows the cross sectional BSE image of the Ti/$Ti_{20}Zr_{20}Cu_{30}Ni_{30}$ /Ti composite joint. It can be seen from Figure 1(a) that the joint was soundly bonded and devoid of imperfections such as cracks and voids. It appears that there was possibly a vigorous interfacial interaction which had occurred during the brazing process and

Preprints (www.preprints.org) | NOT PEER-REVIEWED | Posted: 20 June 2018 doi:10.20944/preprints201806.0309.v1

must have had involved dissolution, diffusion and chemical reaction between the Ti substrate and the molten metallic glass filler. This observation indicates a good wetting and intimate bonding between the substrates and the filler alloy. As shown in Figure 1(a), continuous and sound interfacial reaction layers are formed at the interface between the brazing alloy and the substrates [21, 22]. The reaction layer appeared to have an average thickness of about 4 μm. It had formed at the Ti-alloy/brazed interface. Further, it was thicker than the reaction layer between filler and brazed alloy. The reaction layer appeared to have a thickness of only around 1 μm. As shown in Figure .1a, both reaction layers were primarily composed of Ti.

The corresponding EDX based line scan analysis across 70μm length comprising of the CP-Ti pieces on both sides of brazed joint is shown in Figure 1(b). It shows that the amount of Ti was maximum at the left side interface of the joint and was minimum at about 50 to 65 mm from the same interface. Beyond this point the amount of Ti slightly increased as the right side interface of the joint was approached. Compared to that of Ti, the amounts of Ni, Cu and Zr were a little on the lower side. To elucidate the atomic behavior at the solid/liquid interface, the distribution of the primary elements across the brazing seam was measured by EDX. Thus, the corresponding concentration profiles of Ti, Ni, Cu and Zr are shown in Figures 1(c), (d), (e) and (f), respectively. Similarly, the corresponding EDX based X-ray maps of the elemental distribution of Ti, Zr, Cu and Ni are shown in Figures.1 (a), (b), (c) and (d), respectively. While the presence of Ti was throughout across the brazed joint, there was a relative increase near the left interface region where the reaction had initially started, Figure 1(c). Similarly, the amounts of Ni Figure 1(d) and Cu Figure 1(e) were the minimum at the left interface and grew to their respective maximum positions at about 65 and 50 μm from the left interface [23, 24]. Similarly, the amount of Zr (Figure .1f) was the minimum at the left interface and grew to its maximum positions at about 55 to 60 μm from the left interface. The inhomogeneous and non-uniform distribution of Ni, Cu and Zr across the interface hinted that the diffusion of Zr, Ni and

Preprints (www.preprints.org) | NOT PEER-REVIEWED | Posted: 20 June 2018 doi:10.20944/preprints201806.0309.v1

Cu atoms from the filler into the Ti substrate took place at the solid interface, reducing their concentration in the filler. The quaternary Ti–Zr–Ni–Cu was transformed into a liquid four-membered Ti–Zr–Ni–Cu system with an uncertain composition as a consequence of the intensive interfacial interaction. It can be anticipated that the formation of joint microstructure during the isothermal solidification and cooling of the Ti–Zr–Ni–Cu molten pool were complex. It may be noted that both the element pairs of (Ti and Zr), and (Cu and Ni), have similar atomic radii, crystal structure, and are completely miscible with each other according to the Ti–Zr and Cu–Ni binary phase diagrams [25, 26]. These observations are well corroborated by the X-ray Map data of Ti, Zr, Cu and Ni as shown in Figures .2(a), (b), (c) and (d), respectively.

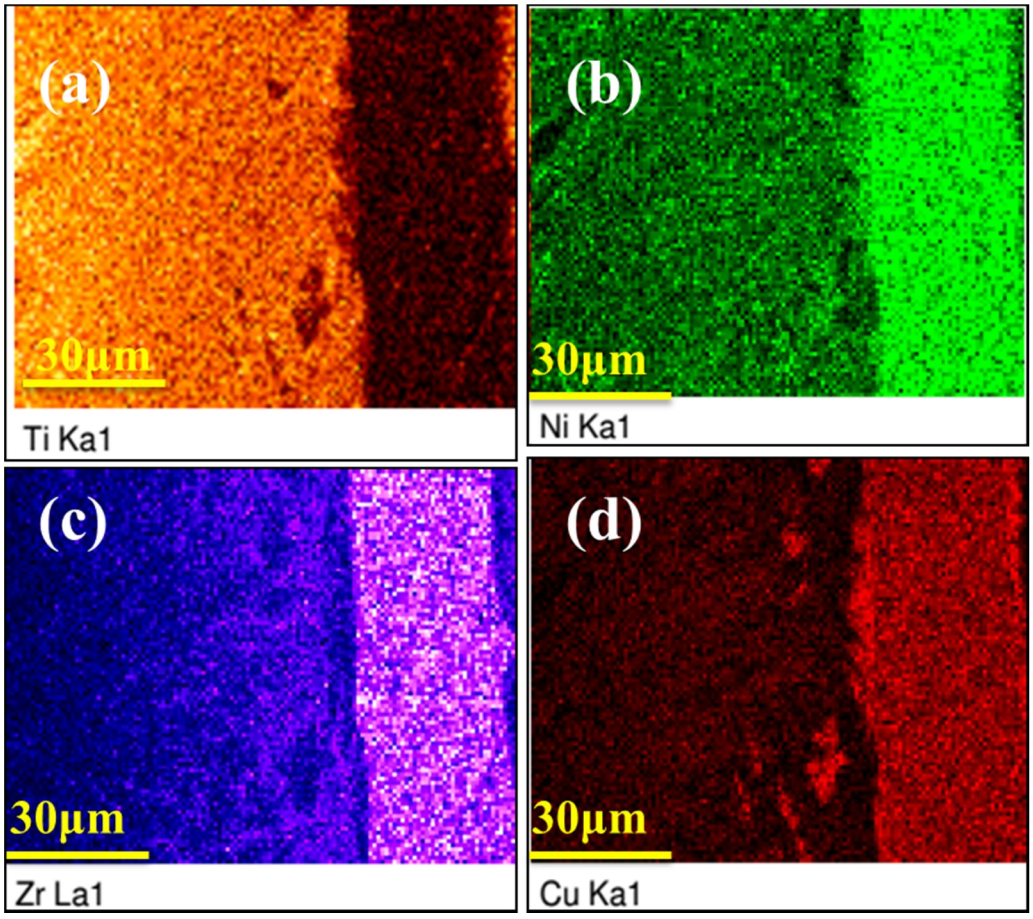

Figure 2. FESEM analyses of Ti/ $Ti_{20}Zr_{20}Cu_{30}Ni_{30}$ /Ti composite joint brazed at 1268 K for a period of 10 min. EDX based X-ray Maps of the distribution of various elements across the brazed joint (a) Ti, (b) Ni, (c) Zr and (d) Cu.

Preprints (www.preprints.org) | NOT PEER-REVIEWED | Posted: 20 June 2018 doi:10.20944/preprints201806.0309.v1

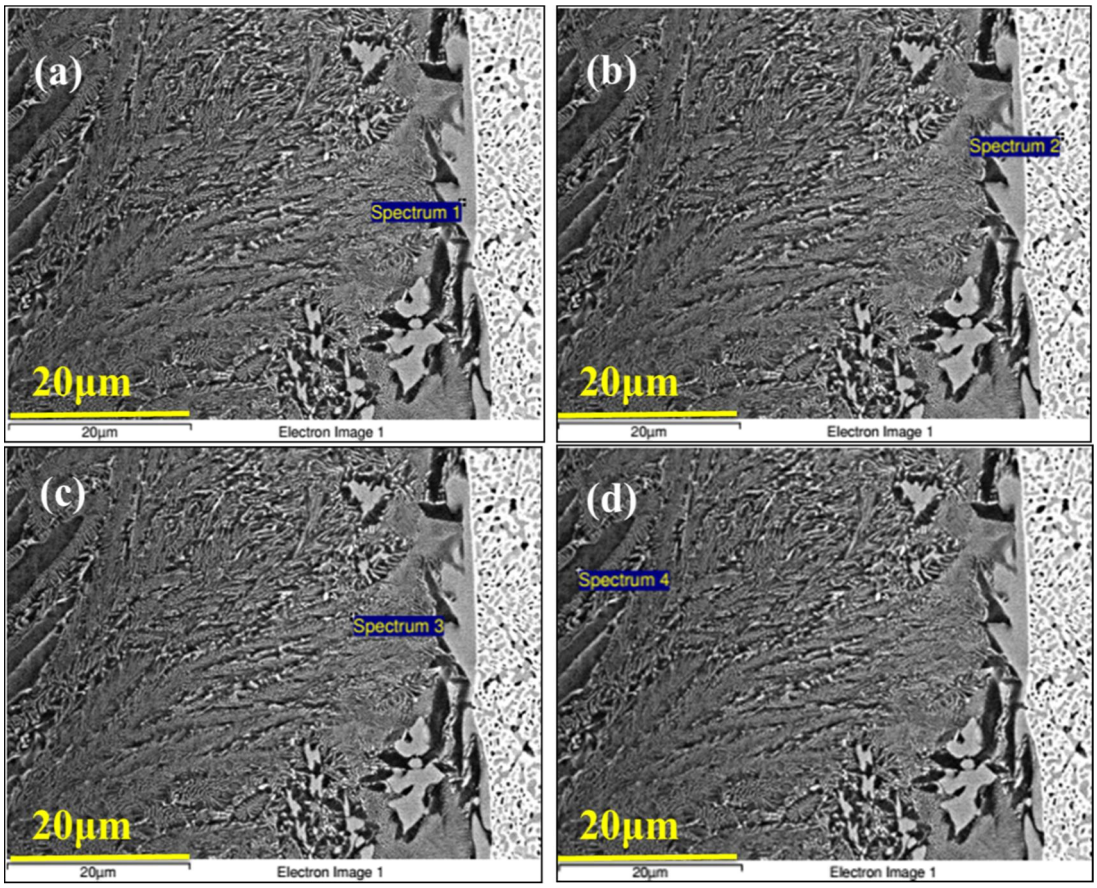

Figure 3. Further FESEM study of the interface microstructures of Ti/ $Ti_{20}Zr_{20}Cu_{30}Ni_{30}$ /Ti composite joint brazed at 1268 K for a period of 10 min: (a) Diffusion zone 1 (b) diffusion zone 2, (c) discontinuous reaction zone and (d) central zone.

The FESEM images of the interface microstructures of Ti/ $Ti_{20}Zr_{20}Cu_{30}Ni_{30}$ /Ti composite joint brazed at 1268 K for a period of 10 min, elucidating the Ti rich diffusion zones 1and 2, the discontinuous reaction zone and the central zone are shown respectively in Figures 3 (a), (b), (c) and (d), respectively. To have an approximate idea of the elemental compositions of these regions, EDX spectrum 1 was taken from Ti_2Cu phase shown in Figure 3 (a), EDX spectrum 2 was taken from the $(Ti, Zr)_2Ni$ rich phase shown in Figure 3 (b), EDX spectrum 3 was taken from the α-Ti rich region shown in Figure 3(c) and EDX spectrum 4 was taken from Ti-rich region shown in Figure 3(d). These EDX spectra are shown in correspondence in Figures. 4 (a), (b), (c) and (d), respectively. The approximate average

Preprints (www.preprints.org) | NOT PEER-REVIEWED | Posted: 20 June 2018 doi:10.20944/preprints201806.0309.v1

chemical compositions obtained from numerous such experiments are shown in Table 1.

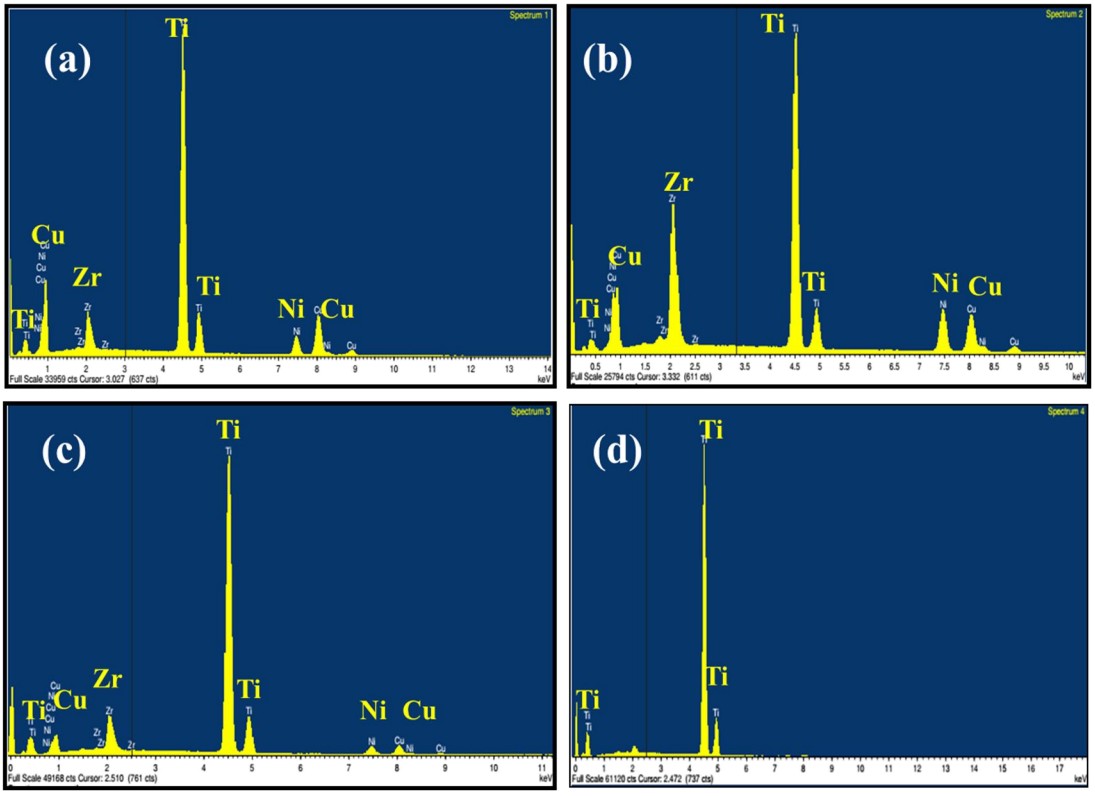

Figure 4. EDX spectra of the interface microstructures of Ti/ $Ti_{20}Zr_{20}Cu_{30}Ni_{30}$ /Ti composite joint brazed at 1268 K for a period of 10 min: (a) Spectrum 1 collected from Diffusion zone 1 shown in Figure 3 (a), (b) Spectrum 2 collected from Diffusion zone 2 shown in Figure 3 (b), (c) Spectrum 3 collected from discontinuous reaction zone shown in Figure 3(c) and (d) Spectrum 4 collected from central zone shown in Figure 3 (d).

Table 1. EDX analyses Based Elemental Chemical Composition Analysis of interface microstructures of Ti/ $Ti_{20}Zr_{20}Cu_{30}Ni_{30}$ /Ti composite joint brazed at 1268 K for a period of 10 min.

Area	Elements (at. %)					
	Ti	Zr	Cu	Ni	Phases	
Spectrum 1	64.45	5.61	21.61	8.33	Ti_2Cu	Ref[27, 33]
Spectrum 2	52.48	16.09	16.22	15.21	$(Ti, Zr)_2Ni$	Ref[28, 34]
Spectrum 3	82.24	6.27	6.60	4.90	α-Ti	Ref[29, 34]
Spectrum 4	100.00	---	---	---	Ti-rich	

Preprints (www.preprints.org) | NOT PEER-REVIEWED | Posted: 20 June 2018 doi:10.20944/preprints201806.0309.v1

Thus, based on the experimental data displayed in Figures 1-4 and Table 1, it appears plausible to suggest the following processes to have occurred during the brazed joint formation. Dissolution of CP-Ti substrate into the brazed melt had possibly resulted in isothermal solidification of the molten brazed and had eventually formed primary β-Ti during brazing. The residual melt was solidified via eutectic reaction upon the cooling cycle of brazing. Based on the data of Table 1, the eutectic consisted most probably of Ti_2Cu, $(Ti,Zr)_2Ni$, α-Ti and Ti-rich phases as displayed in Figures 3(a-d) and Figures 4 (a-d). According to related binary alloy phase diagrams, the β-Ti is completely soluble with Zr [30-34].

Maximum solubilities of Cu and Ni in the β-Ti are 28.5 and 28 at. %, respectively. In contrast, Cu and Ni are dissolved in α-Ti up to 1.4 and 1.4 at. %, respectively. These values are significantly lower than their respective solubilities in β-Ti. Both Cu and Ni are hence well known to be stabilizers of the β phase in CP-Titanium. On cooling to room temperature formation of both β-phase and intermetallic compounds may take place. Accordingly, decomposition of the β-Ti phase might have most probably proceeded via eutectoid solid-state transformation upon the cooling cycle of brazing. The eutectoid of Ti_2Cu, $(Ti, Zr)_2$ Ni, α-Ti and Ti-rich phases might therefore have had formed at room temperature in the earlier β-Ti grains of the brazed joint. Higher brazing temperature resulted possibly in higher volume fraction of the β-Ti in the joint. This process had greatly enhances the depletion rates of Cu, Ni, and Zr from the brazed melt into CP-Ti substrate during brazing. Because Cu, Ni, and Zr are all dissolved in the β-Ti, isothermal solidification of brazed melt during brazing resulted in formation of only β-Ti in the joint. Thus, the eutectic of eutectoid of Ti_2Cu, $(Ti, Zr)_2$ Ni, α-Ti and Ti-rich phases had most likely disappeared from the brazed zone. The β-Ti alloyed

Preprints (www.preprints.org) | NOT PEER-REVIEWED | Posted: 20 June 2018 doi:10.20944/preprints201806.0309.v1

with Cu, Ni, and Zr was therefore most likely to have had transformed to fine eutectoid of eutectoid of Ti_2Cu, $(Ti, Zr)_2Ni$, α-Ti and Ti-rich phases upon the subsequent cooling cycle of brazing. It is expected that the disappearance of coarse eutectic intermetallic compounds from the brazed zone is beneficial for enhancing the bond strength of the joint.

3.2 Microstructure analysis of Ti/$Ti_{20}Zr_{20}Cu_{20}Ni_{40}$/Ti composite joint brazed at 1277 K for a period of 10 min

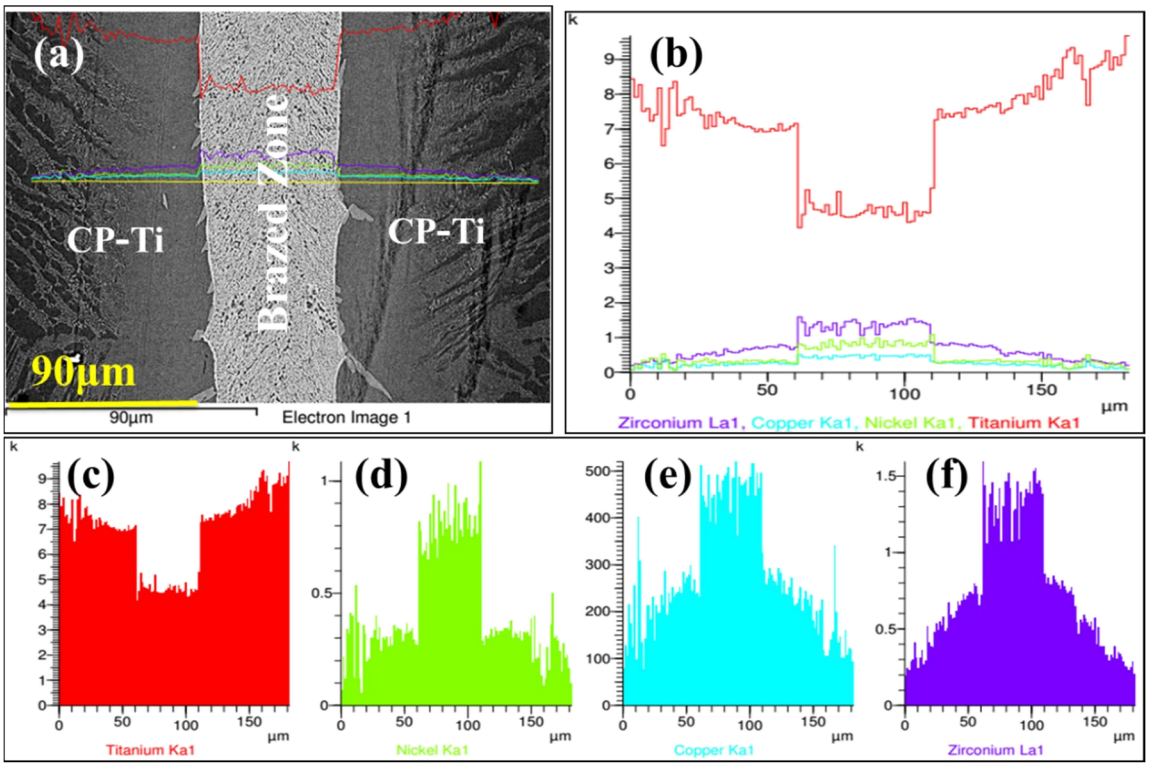

Figure 5. FESEM analysis of Ti/ $Ti_{20}Zr_{20}Cu_{20}Ni_{40}$ /Ti composite joint brazed at 1004°C for a period of 10 min (a) Cross sectional BSE Image (b) corresponding EDX based line scan analysis across 90 µm length comprising the CP-Ti pieces on both sides of brazed joint, corresponding concentration profiles of elements :(c)Ti, (d) Ni (e) Cu and (f) Zr.

The continuous and interfacial reaction layers (appeared to have an average thickness of about 40 µm) formed at the interface between the brazing alloy and substrates are indicated in Figure 5(a). The corresponding EDX based line scan analysis across 180 µm length comprising of the CP-Ti pieces on both sides of brazed joint is depicted in Fig 5(b). It shows that the amount of Ti was maximum at the vicinity of interface on both sides but it was

Preprints (www.preprints.org) | NOT PEER-REVIEWED | Posted: 20 June 2018 doi:10.20944/preprints201806.0309.v1

minimum at the region from about 60 to 110 μm from the left interface [16]. Similarly, the corresponding EDX based X-ray maps of the elemental distribution of Ti, Zr, Cu and Ni are shown in Figures 6(a), (b), (c) and (d), respectively. While the presence of Ti was throughout across the brazed joint, there was a relative increase near the interface region where the reaction had initially started, Figure 5(c). Similarly, the amounts of Ni Figure 5(d), Cu Figure 5(e) and Zr Figure 5(f) were more at the centre of the brazed joint but became slightly lesser at the vicinity of the interface. These observations are in good agreement with the X-ray Map data of Ti, Zr, Cu and Ni (*cf*. Figures 6 a-d). The EDX spectra of $NiTi_2$, $(Ti, Zr)_2 Ni$, β-(Ti, Zr) and Ti-rich phases are shown in Figures.7 (a), (b), (c) and (d), respectively. These EDX spectra with corresponding elemental compositions shown in Figures. 8 (a), (b), (c) and (d), respectively and given in Table 2.

The solubilities of Cu and Ni in the β-Ti phase are maximum at 18.5 and 38 at. %, respectively. In contrast, Cu and Ni are dissolved in α-Ti up to 0.4 and 2.4at. %, respectively. Thus, the eutectic of $NiTi_2$, $(Ti,Zr)_2Ni$, β-(Ti,Zr) and Ti-rich phases had most likely disappeared from the brazed zone [27, 28].

Table 2. EDX analyses based elemental chemical composition analysis of interface microstructures of Ti/ $Ti_{20}Zr_{20}Cu_{20}Ni_{40}$ /Ti composite brazing joint at 1277 K for a period of 10 min

Area	Elements (at. %)					
	Ti	Zr	Cu	Ni	Phases	
Spectrum 1	52.35	16.37	10.77	20.51	$NiTi_2$	Ref[34]
Spectrum 2	59.75	6.75	18.62	14.88	$(Ti,Zr)_2Ni$	Ref[34]
Spectrum 3	80.48	6.97	5.40	7.15	β(Ti, Zr)	Ref[34]
Spectrum 4	100.00	---	---	---	Ti-rich	

Preprints (www.preprints.org) | NOT PEER-REVIEWED | Posted: 20 June 2018 doi:10.20944/preprints201806.0309.v1

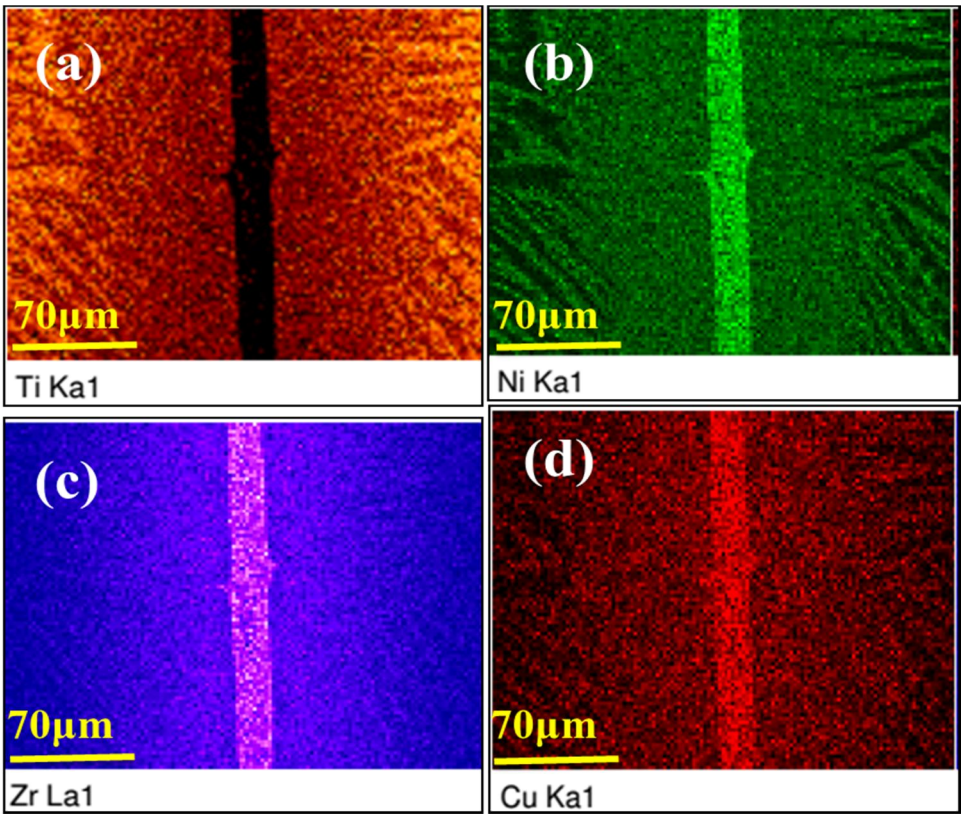

Figure 6. FESEM analysis of Ti/ $Ti_{20}Zr_{20}Cu_{20}Ni_{40}$ /Ti composite joint brazed at 1277 K for a period of 10 min. EDX based X-ray Maps of the distriution of various elements across the brazed joint (a) Ti, (b)Ni, (c) Zr and (d) Cu.

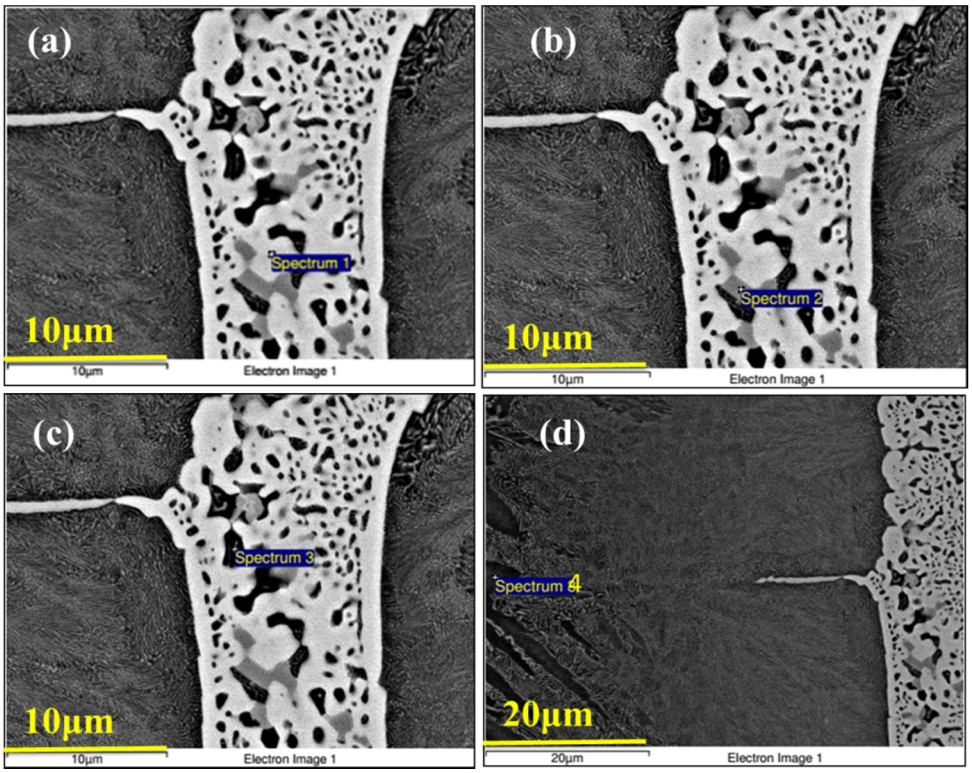

Figure 7. Further FESM study of the interface microstructures of Ti/ $Ti_{20}Zr_{20}Cu_{20}Ni_{40}$ /Ti composite joint brazed at 1277 K for a period of 10 min: (a)

Preprints (www.preprints.org) | NOT PEER-REVIEWED | Posted: 20 June 2018 doi:10.20944/preprints201806.0309.v1

Diffusion zone 1 (b) diffusion zone 2, (c) discontinuous reaction zone and (d) central zone.

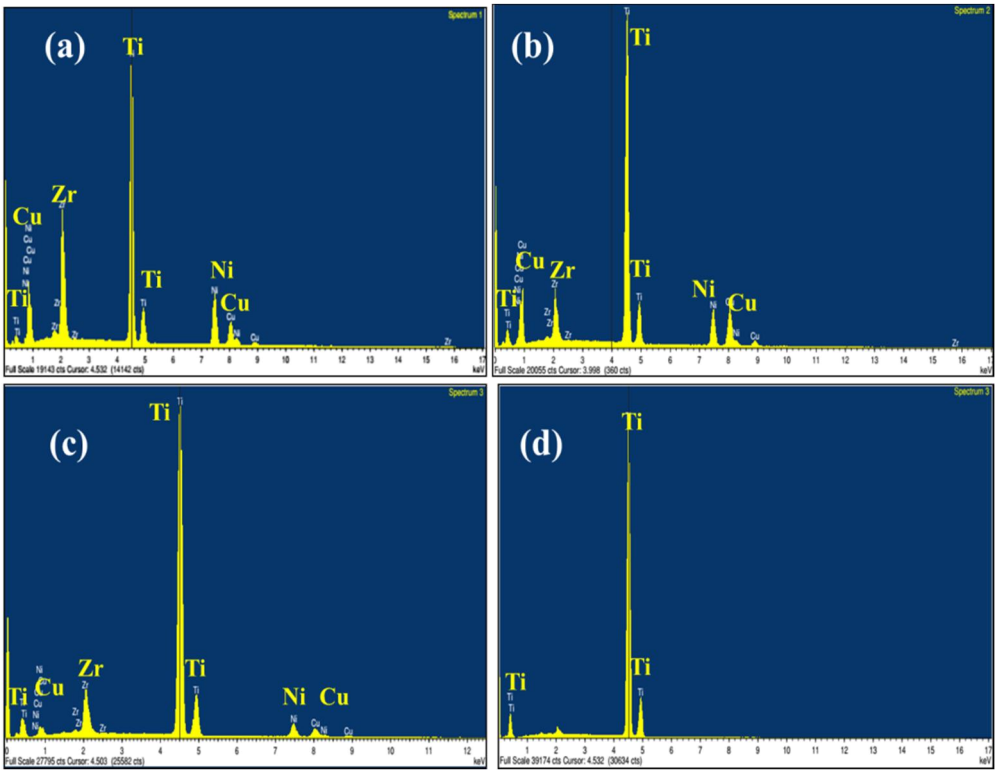

Figure 8. EDX spectra of the interface microstructures of Ti/ $Ti_{20}Zr_{20}Cu_{20}Ni_{40}$ /Ti composite joint brazed at 1277 K for a period of 10 min: (a) Spectrum 1 collected from Diffusion zone 1 shown in Figure 6 (a), (b) Spectrum 2 collected from Diffusion zone 2 shown in Figure 6 (b), (c) Spectrum 3 collected from discontinuous reaction zone shown in Figure 6 (c) and (d) Spectrum 4 collected from central zone shown in Figure 6(d).

Preprints (www.preprints.org) | NOT PEER-REVIEWED | Posted: 20 June 2018 doi:10.20944/preprints201806.0309.v1

3.3 Microstructure analysis of Ti/$Ti_{20}Zr_{20}Cu_{10}Ni_{50}$/Ti composite joint brazed at 1279 for a period of 10 min

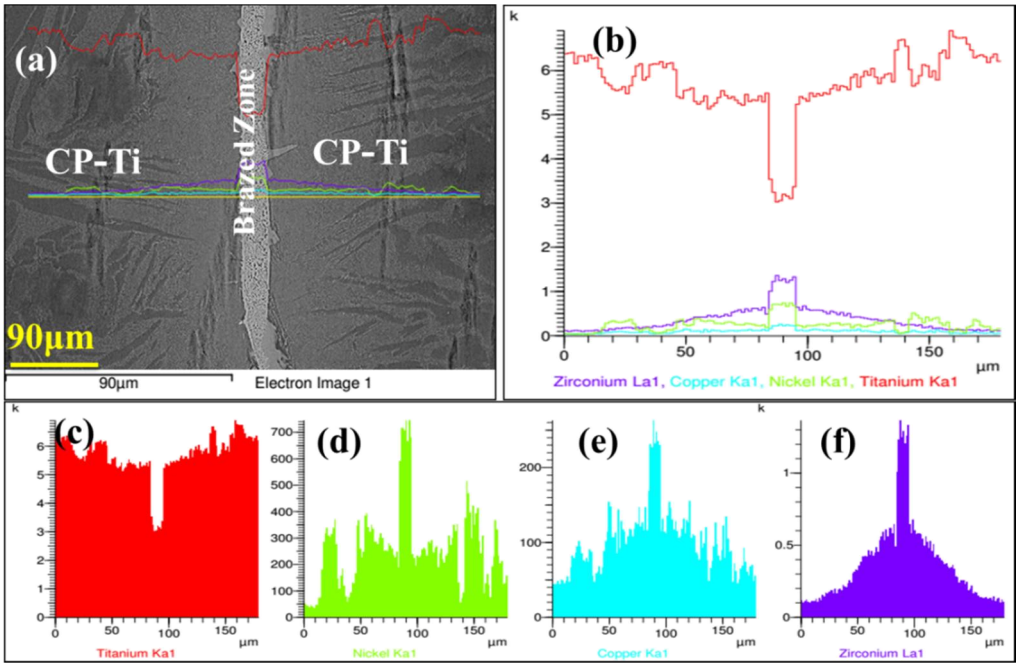

Figure 9. FESEM analysis of Ti/ $Ti_{20}Zr_{20}Cu_{10}Ni_{50}$ /Ti composite joint brazed at 1279 K for a period of 10 min (a) Cross sectional BSE Image (b) corresponding EDS based line scan analysis across 90 µm length comprising the CP-Ti pieces on both sides of brazed joint, corresponding concentration profiles of elements :(c)Ti, (d)Ni (e) Cu and (f) Zr.

Continuous and sound interfacial reaction layers (of thickness about 40 µm) are formed at the interface between the brazing alloy and the substrates. As earlier, both reaction layers were primarily composed of Ti, shown in Figure 9 (a). The corresponding EDX based line scan analysis across 180 µm length comprising of the CP-Ti pieces on both sides of brazed joint is shown in Figure 9 (b). It shows that the amount of Ti was maximum at the vicinity of interface on both sides, but it was minimum at the region from about 85 to 95 µm from the left interface. Compared to that of Ti, the amounts of Ni, Cu and Zr were a little on the lower side. To elucidate the atomic behaviour at the solid/liquid interface, the distribution of the primary elements across the brazing seam was measured by EDX.

Preprints (www.preprints.org) | NOT PEER-REVIEWED | Posted: 20 June 2018 doi:10.20944/preprints201806.0309.v1

Thus, the corresponding concentration profiles of Ti, Ni, Cu and Zr are shown in Figure 9(c), (d), (e) and (f), respectively. Similarly, the corresponding EDX based X-ray maps of the elemental distribution of Ti, Zr, Cu and Ni are shown in Figure 10 (a), (b), (c) and (d), respectively. While the presence of Ti was throughout across the brazed joint, there was a relative increase near the interface region where the reaction had initially started, Figure 9 (c). Similarly, the amounts of Ni Figure 9 (d), Cu Figure 9 (e) and Zr Figure 9 (f) were more at the centre (e.g., at about 85 to 95 μm from the left interface) of the brazed joint but became slightly lesser at the vicinity of the interface. These observations are well corroborated by the X-ray Map data of Ti, Zr, Cu and Ni as shown in Figure 10 (a), (b), (c) and (d), respectively. The Ti rich diffusion (4,5), discontinuous reaction (3) and central zones (1,2) are shown in Figures 11 (a), (b), (c), (d) and (e), respectively. The EDX spectra of $NiTi_2$, Cu_2(Ni, Zr), NiTi, α-Ti and Ti-rich phases shown in Figures. 12 (a), (b), (c), (d) and (e), respectively and the approximate average chemical compositions obtained from numerous such experiments are shown in Table 3. The solubilities of Cu and Ni in the β-Ti phase are maximum at 48.5 and 8 at.%, respectively. In contrast, Cu and Ni are dissolved in α-Ti phase up to 2.4 and 1.4 at.%, respectively.

Preprints (www.preprints.org) | NOT PEER-REVIEWED | Posted: 20 June 2018 doi:10.20944/preprints201806.0309.v1

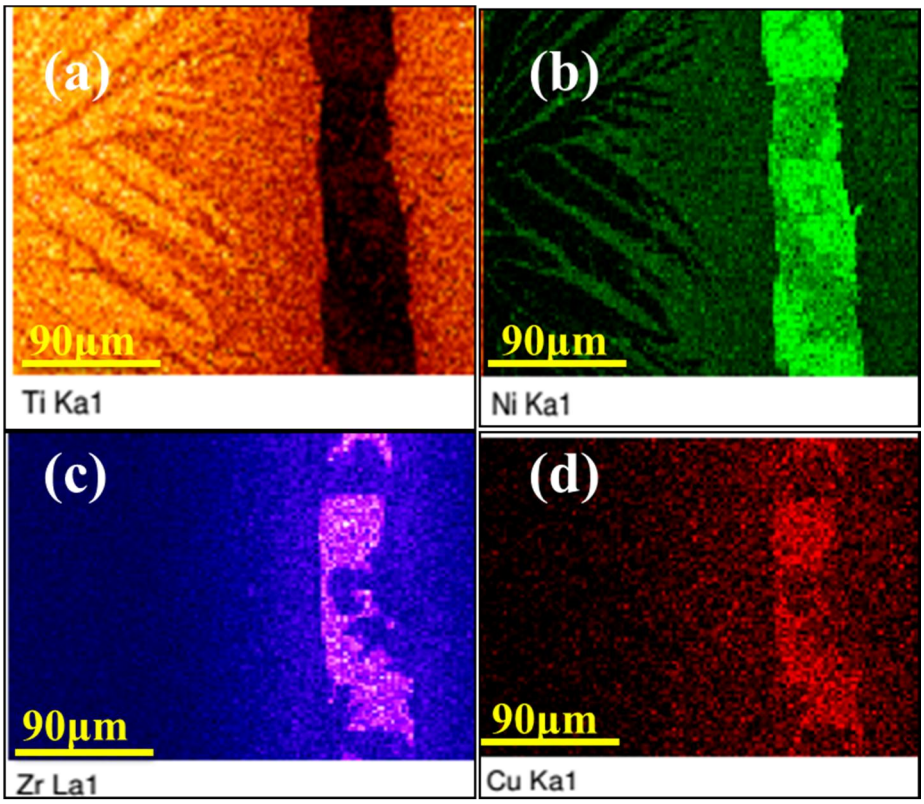

Figure 10. FESEM analysis of Ti/ $Ti_{20}Zr_{20}Cu_{10}Ni_{50}$ /Ti composite joint brazed at 1279 K for a period of 10 min. EDX based X-ray Maps of the distribution of various elements across the brazed joint (a) Ti, (b)Ni, (c) Zr and (d) Cu.

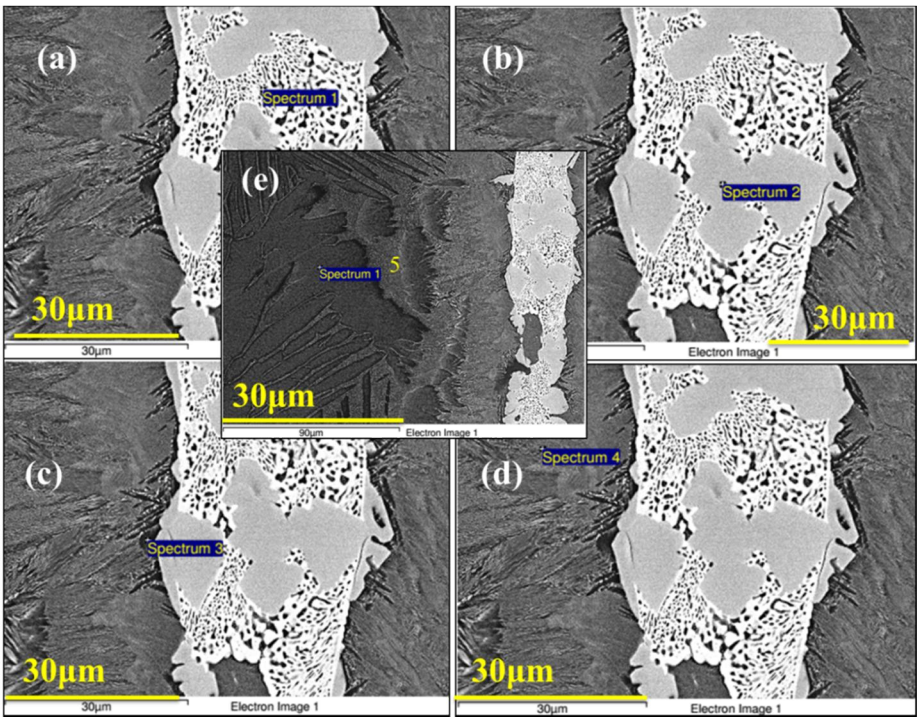

Figure 11. Further FESM study of the interface microstructures of Ti/ $Ti_{20}Zr_{20}Cu_{10}Ni_{50}$ /Ti composite joint brazed at 1279 K for a period of 10 min: (a) Diffusion zone 1 (b) diffusion zone 2, (c) diffusion zone 3, (d) discontinuous reaction zone and (e) central zone.

Preprints (www.preprints.org) | NOT PEER-REVIEWED | Posted: 20 June 2018 doi:10.20944/preprints201806.0309.v1

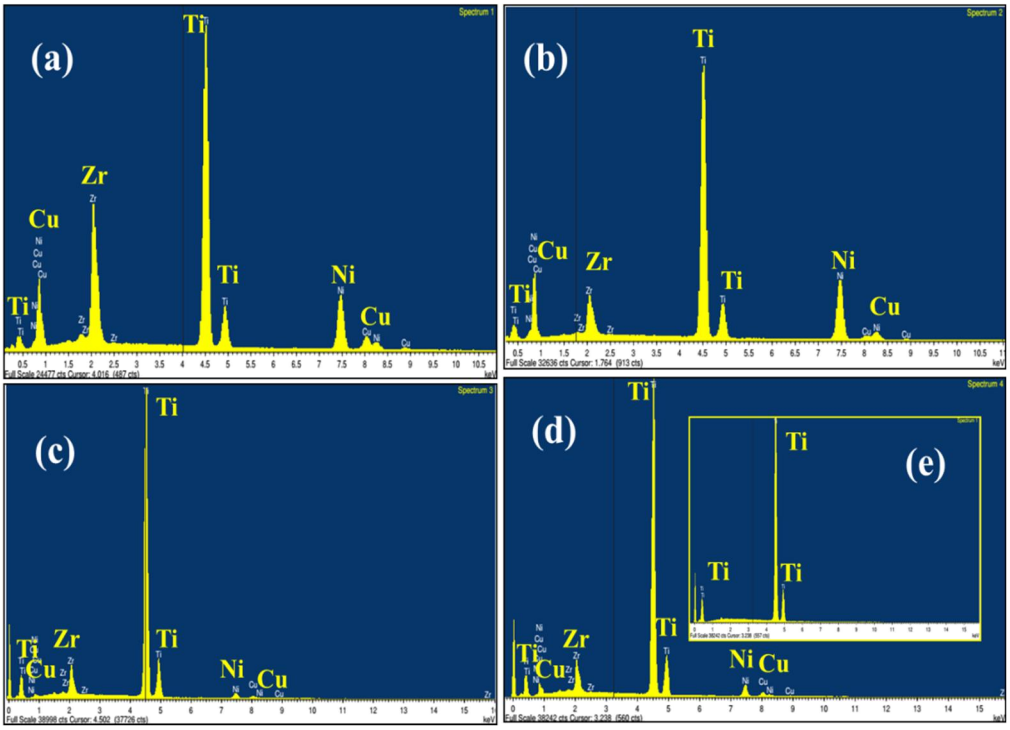

Figure 12. EDX spectra of the interface microstructures of Ti/$Ti_{20}Zr_{20}Cu_{10}Ni_{50}$/Ti composite joint brazed at 1279 K for a period of 10 min: (a) Spectrum 1 collected from Diffusion zone 1 shown in Figure 11 (a), (b) Spectrum 2 collected from Diffusion zone 2 shown in Figure 11 (b), (c) Spectrum 3 collected from discontinuous reaction zone shown in Figure 11(c) and (d) Spectrum 4, 5 collected from central zone shown in Figure 11 (e).

Table 3. EDX analyses based elemental chemical composition analysis of interface microstructures of Ti/$Ti_{20}Zr_{20}Cu_{10}Ni_{50}$/Ti composite brazing joint at 1279 K for a period of 10 min

Area	Elements (at. %)					
	Ti	Zr	Cu	Ni	Phases	
Spectrum 1	56.69	16.50	5.86	20.95	$NiTi_2$	Ref[34]
Spectrum 2	60.91	6.37	2..16	30.57	Cu_2(Ni, Zr)	Ref[33]
Spectrum 3	89.55	5.51	1.58	3.36	NiTi	Ref[34]
Spectrum 4	84.38	5.62	2.81	7.19	α-Ti	Ref[34]
Spectrum 5	100.00	---	---	---	Ti-rich	

Preprints (www.preprints.org) | NOT PEER-REVIEWED | Posted: 20 June 2018 doi:10.20944/preprints201806.0309.v1

4. Annealing studies of ribbons

The XRD spectra shown in Figure. 13 confirmed that annealing at 758 K for a period of 30 min, produced the crystalline phases NiTi, $NiTi_2$, Ni_4Ti_3, $CuNi_2Ti$, and Ni_2Ti, $NiTi_{0.8}Zr_{0.2}$ in the $Ti_{20}Zr_{20}Cu_{30}Ni_{30}$ metallic glass ribbons [16]. The XRD spectra shown in Fig. 14 confirmed that annealing at 778 K for a period of 30 min, produced the crystalline phases NiTi, $NiTi_2$, Ni_2Ti, Cu_8Zr_3, Ni_4Ti_3, $CuNi_2Ti$, Ni_2Ti, and $NiTi_{0.8}Zr_{0.2}$ in the $Ti_{20}Zr_{20}Cu_{20}Ni_{40}$ metallic glass ribbons. The XRD spectra shown in Figure 15 confirmed that annealing at 783 K for a period of 30 min produced the crystalline phases $NiTi_2$, Ni_2Ti, NiTi, Ni_4Ti_3, and $CuNi_2Ti$ in the $Ti_{20}Zr_{20}Cu_{10}Ni_{50}$ metallic glass ribbons. The annealing temperature corresponded to the onset of crystallization temperature (T_x) of the exothermic peak on DSC curves.

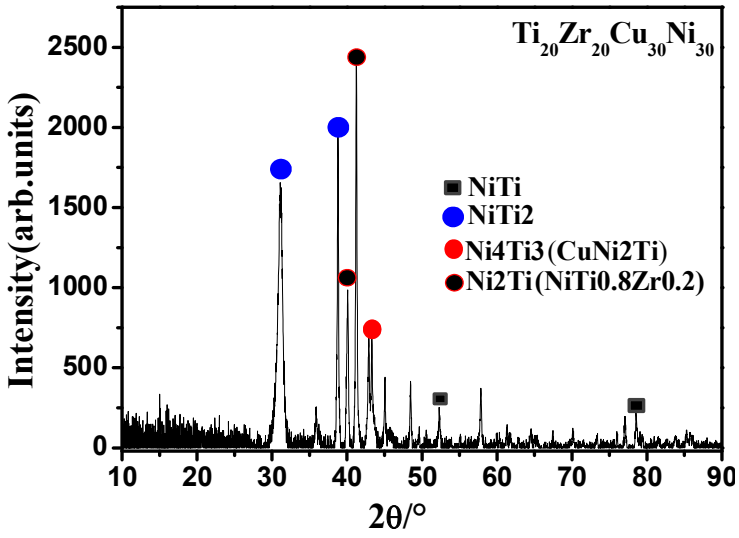

Figure 14. XRD spectra of the $Ti_{20}Zr_{20}Cu_{30}Ni_{30}$ Metallic glass Ribbons annealed at 758 K for a period of 30 min.

Preprints (www.preprints.org) | NOT PEER-REVIEWED | Posted: 20 June 2018 doi:10.20944/preprints201806.0309.v1

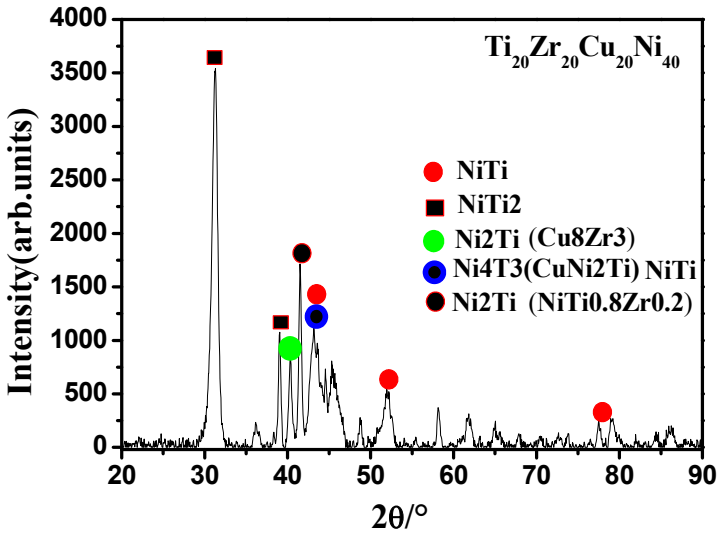

Figure 14. XRD spectra of the $Ti_{20}Zr_{20}Cu_{20}Ni_{40}$ Metallic glass Ribbons annealed at 778 for a period of 30 min.

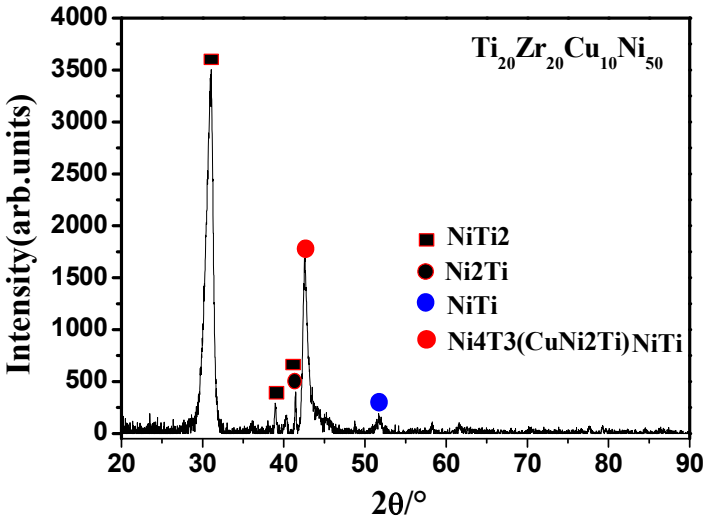

Figure 15. The $Ti_{20}Zr_{20}Cu_{10}Ni_{50}$ metallic glass ribbon annealed at 783 K for a period of 30 min, and the corresponding XRD spectrum.

Preprints (www.preprints.org) | NOT PEER-REVIEWED | Posted: 20 June 2018 doi:10.20944/preprints201806.0309.v1

3.8 Transmission Electron Microscopy

The Figures16.(a-c) represent the bright field (BF), dark field (DF) and corresponding SAED, respectively for the$Ti_{20}Zr_{20}Cu_{50}Ni_{10}$ metallic glass ribbon annealed at 758 K for a period of 30 min. Table 4 presents the corresponding data on composition analysis of the annealed $Ti_{20}Zr_{20}Cu_{30}Ni_{30}$ metallic glass ribbon.

These results e.g., figures. 16 (c) and Table 4 corroborated with the corresponding XRD data figure.13. The homogeneous distribution of the various nanocrystalline phases in amorphous matrix has been shown in figsure.16 (a) and (b). Existence of these nanocrystalline phases were confirmed from both the XRD data figure. 13 and the compositional analysis data obtained from the TEM studies Table 4. The range of the size of spherical features in the dark field image figure 16 (b) was about 10 to 100 nm while the average feature size was about 50 nm figure 16 (a).

The BF, DF and corresponding SAED pattern of the annealed $Ti_{20}Zr_{20}Cu_{20}Ni_{40}$ metallic glass at 778 K for a period of 30 min are shown in Figures 17(a), (b) and (c), respectively. Table 5 presents the corresponding data on compositional analysis of the same annealed ribbon. These results e.g., figure. 17(c) and Table 5 corroborated with the corresponding XRD data (Figure. 14).

The homogeneous distribution of the various nanocrystalline phases in amorphous matrix has also been observed (Figures. 17 (a) and (b)). Existence of the nanocrystalline phases were confirmed from both the XRD data figure. 14 and the compositional analysis data obtained from the TEM studies Table 5. The range of the size of spherical features in the dark field image figure 17 (b) was about 10 to 100 nm [18, 19].

Preprints (www.preprints.org) | NOT PEER-REVIEWED | Posted: 20 June 2018 doi:10.20944/preprints201806.0309.v1

The same phenomena followed for BF, DF and the corresponding SAED patterns of the annealed metallic glass ribbons viz., $Ti_{20}Zr_{20}Cu_{10}Ni_{50}$ (annealed at 783 K). The corresponding data on compositional analysis of the above three glasses are also shown in TEM studies Tables 4-6. Existence of these nanocrystallie phases were confirmed from both the XRD data (Figures. 16-18).

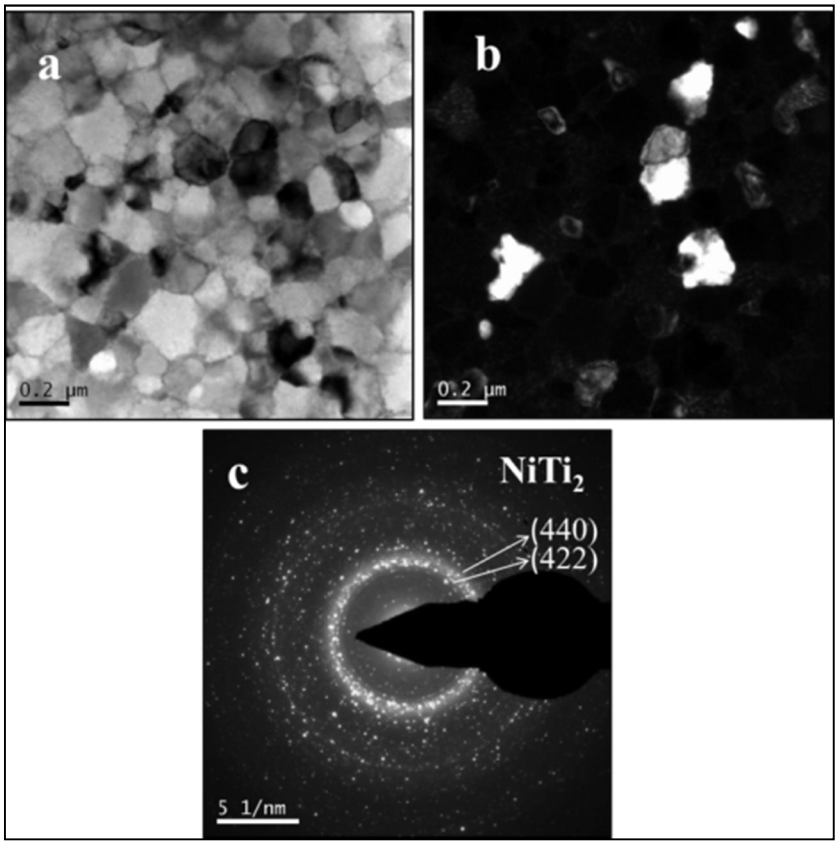

Figure 16. The annealed ribbon of $Ti_{20}Zr_{20}Cu_{30}Ni_{30}$ metallic glass at 758 K for a period of 30 min and the corresponding TEM images: (a)-(c): BF image, DF image and selected area of electron diffraction pattern (SAED), respectively.

Table 4. The analytical composition of the $Ti_{20}Zr_{20}Cu_{30}Ni_{30}$ metallic glass ribbon (annealed at 758K for a period of 30 min)

Elements (at. %)				
Ti	**Zr**	**Cu**	**Ni**	**Phases**
18.34	23.28	26.74	31.63	NiTi

Preprints (www.preprints.org) | NOT PEER-REVIEWED | Posted: 20 June 2018 doi:10.20944/preprints201806.0309.v1

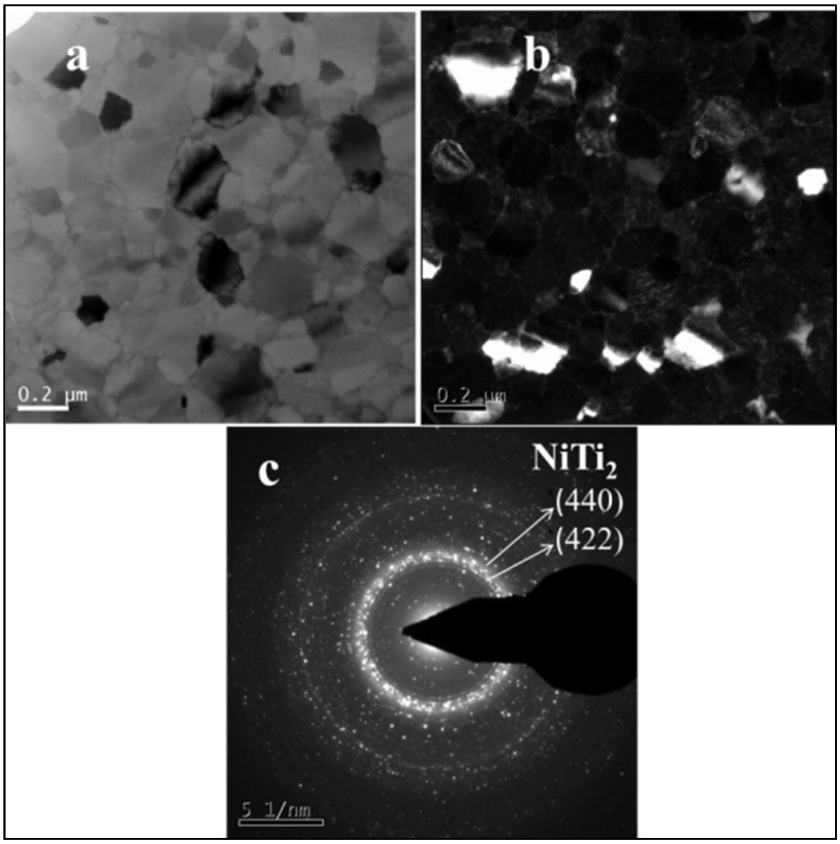

Figure 17. The annealed ribbon of $Ti_{20}Zr_{20}Cu_{20}Ni_{40}$ metallic glass at 778 K for a period of 30 min and the corresponding TEM images: (a)-(c): BF image, DF image and selected area of electron diffraction pattern (SAED), respectively.

Table 5. The analytical composition of the $Ti_{20}Zr_{20}Cu_{20}Ni_{40}$ metallic glass ribbon (annealed at 778K for a period of 30 min)

Elements (at. %)				
Ti	**Zr**	**Cu**	**Ni**	**Phases**
18.00	19.30	17.77	44.91	NiTi2

Preprints (www.preprints.org) | NOT PEER-REVIEWED | Posted: 20 June 2018 doi:10.20944/preprints201806.0309.v1

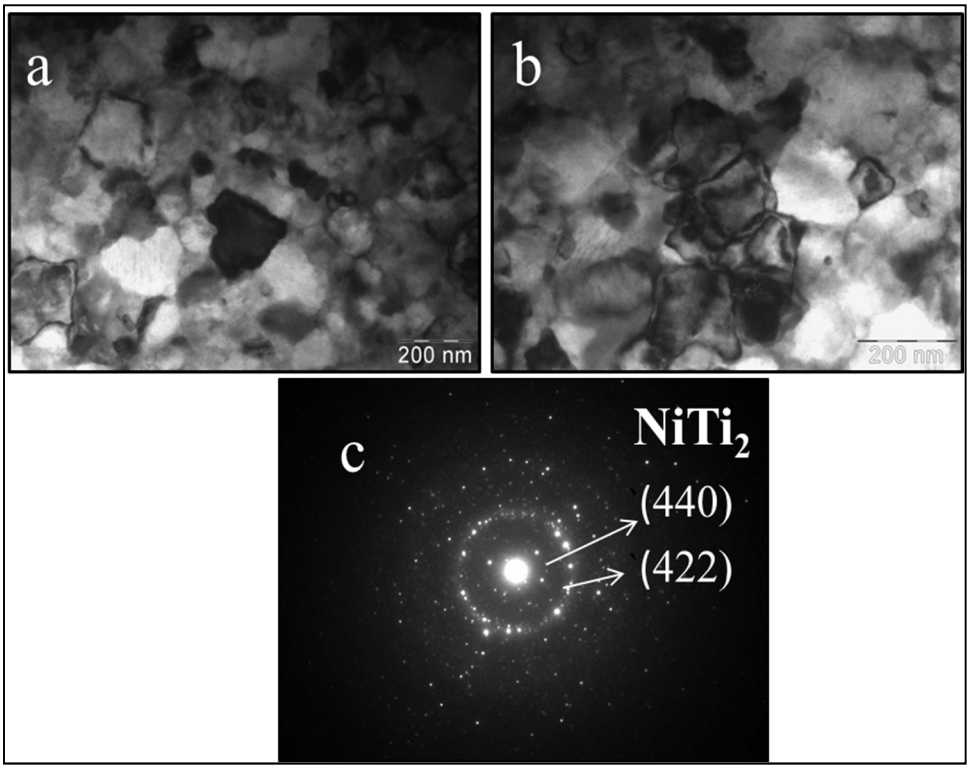

Figure 18. The annealed ribbon of $Ti_{20}Zr_{20}Cu_{10}Ni_{50}$ metallic glass at 778 K for a period of 30 min and the corresponding TEM images: (a)-(c): BF image, DF image and selected area of electron diffraction pattern (SAED), respectively.

Table 6. The analytical composition of the $Ti_{20}Zr_{20}Cu_{10}Ni_{50}$ metallic glass ribbon (annealed at 783K for a period of 30 min)

Elements (at. %)				
Ti	**Zr**	**Cu**	**Ni**	**Phases**
17.21	22.97	9.75	50.06	NiTi2

Preprints (www.preprints.org) | NOT PEER-REVIEWED | Posted: 20 June 2018 doi:10.20944/preprints201806.0309.v1

Conclusions

A. The microstructural analysis for brazed samples of $Ti_{20}Zr_{20}Cu_{60-x}Ni_x$ (x=30, 40 and 50) metallic glasses with CP-Ti alloy pieces were respectively braze joined using metallic glass ribbon fillers of compositions $Ti_{20}Zr_{20}Cu_{60-x}Ni_x$ (x=30, 40 and 50) at 1268 , 1277 K and 1279 K for a period of 10 min. Based on extensive studies of FESEM, EDX line scans, EDX spectrum analysis and Elemental X-Ray Mapping by EDX it was found that depending on the combination of filler composition, brazing condition and cooling cycle of the brazing processes the corresponding joints were characterized by microstructure formed by fine lamellar eutectoids of (a) $NiTi_2$, Ti_2Cu , α-Ti and Ti-rich phases, (b) $NiTi_2$, $(Ti, Zr)_2Ni$, β(Ti, Zr) and Ti-rich phases and (c) $NiTi_2$, $Cu_2(Ni, Zr)$, NiTi ,α-Ti and Ti-rich phases; in correspondence.

B. The XRD spectra shown in produced the crystalline phases NiTi, $NiTi_2$, Ni_4Ti_3, $CuNi_2Ti$, and Ni_2Ti, $NiTi_{0.8}Zr_{0.2}$ in the $Ti_{20}Zr_{20}Cu_{30}Ni_{30}$ metallic glass, NiTi, $NiTi_2$, Ni_2Ti, Cu_8Zr_3, Ni_4Ti_3, $CuNi_2Ti$, Ni_2Ti, and $NiTi_{0.8}Zr_{0.2}$ in the $Ti_{20}Zr_{20}Cu_{20}Ni_{40}$ metallic glass and $NiTi_2$, Ni_2Ti, NiTi, Ni_4Ti_3, and $CuNi_2Ti$ in the $Ti_{20}Zr_{20}Cu_{10}Ni_{50}$ metallic glass ribbons.

C. The $Ti_{20}Zr_{20}Cu_{30}Ni_{30,}$ $Ti_{20}Zr_{20}Cu_{20}Ni_{40}$ and $Ti_{20}Zr_{20}Cu_{10}Ni_{50}$ metallic glass ribbons annealed at 758, 778 and 783 K, respectively for a period of 30 min produced the crystalline phases of NiTi, $NiTi_2$ and $NiTi_{2,}$ respectively. The homogeneous distribution of the various nanocrystalline phases in the amorphous matrix and the existence of these nanocrystallie phases were confirmed from the XRD, TEM data and compositional analysis data obtained from the EDAX studies.

Acknowledgements

The authors gratefully acknowledge the support of this research through the fund provided by the University Grants Commission-Rajiv Gandhi National Fellowship (UGC-RGNF). AKB thanks the Indian National Science Academy (INSA), New Delhi for the support through Senior Scientist Platinum jubilee Fellowship, UGC-DAE-CSR (Mumbai) through project CRS-M199. And also the authors would like to express their grateful thanks to Director, CSIR-CGCRI.

References

1. Y. Zhao et al. Interfacial microstructure and mechanical properties of porous-Si3N4 ceramic and Ti-Al alloy joints vacuum brazed with Ag-Cu filler, Ceramics International 43 (2017) 9738–9745.
2. J. Cao, Xiangyu Dai, Jiaqi Liu, Xiaoqing Si, Jicai Feng, Relationship between microstructure and mechanical properties of TiAl/ Ti2AlNb joint brazed using Ti-27Co eutectic filler metal , Materials and Design 121 (2017) 176–184
3. Qiwen Qiu, Ying Wang, Zhenwen Yang, Xin Hu, Dongpo Wang, Microstructure and mechanical properties of TiAl alloy joints vacuum brazed with Ti–Zr–Ni–Cu brazing powder without and with Mo additive, Materials and Design 90 (2016) 650–659.
4. B.B. Medeiros et al. / Journal of Non-Crystalline Solids 425 (2015) 103–109.
5. M. Kazunari, I. Yuki, M. Hirotaka, and M. Hiroyuki: Scripta Mater, vol. 68, (2013), pp. 777–80.
6. X. L. Bian, G. Wang, K. C. Chan, J. L. Ren, Y. L. Gao, Appl. Phys. Lett. 103, 101907 (2013).

7. E. Ganjeh, H. Sarkhosh, M.E. Bajgholi, H. Khorsand, M.H. Ghaffari, Increasing Ti–6Al–4V brazed joint strength equal to the base metal by Ti and Zr amorphous filler alloys Materials characterization 71(2012)31-40.
8. Elrefaey A, Tillmann W. brazing of titanium to steel with different filler metals: analysis and comparison. J Mater Sci 45 (2010): 4332–8.
9. Lee JG, Choi YH, Lee JK, Lee GJ, Lee MK, Rhee CK. Low-temperature brazing of titanium by the application of a Zr–Ti–Ni–Cu–Be Bulk Metallic Glass (BMG) alloy as a filler. Intermetallics (2010); 18:70–3.
10. Y. Huang, Y.L. Chiu, J. Shen, J.J.J. Chen, J. Sun, Nanoindentation study of Ti-based metallic glasses, J. Alloys Compd. 479 (2009) 121–128.
11. Elrefaey A, Tillmann W. Correlation between microstructure, mechanical properties, and brazing temperature of steel to titanium joint. J Alloys Compd 487 (2009); 639–45.
12. N.K. Mukhopadhyay, A. Belger, P. Paufler, D.H. Kim, Nanoindentation studies on Cu–Ti–Zr–Ni–Si–Sn bulk metallic glasses, Mater. Sci. Eng. A 449–451 (2007) 954–957.
13. Y.J. Yang, F.W. Kang, D.W. Xing, J.F. Sun, Q.K. Shen, J. Shen, Formation and mechanical properties of bulk Cu–Ti–Zr–Ni metallic glasses with high glass forming ability, Trans. Nonferrous Met. Soc. China 17 (2007) 16–20.
14. Chang CT, Wu ZY, Shiue RK, Chang CS. Infrared brazing Ti–6Al–4V and SP-700 alloys using the Ti–20Zr–20Cu–20Nibraze alloy. Mater Lett (2007); 61:8425.

15. Materials Science International Team M. Ternary alloy systems: phase diagrams, crystallographic and thermodynamic data, V 11. Berlin, Germany: Springer; (2007).

16. Hong IT, Koo CH. Microstructural evolution and shears strength of brazing C103 and Ti–6Al–4V using Ti–20Cu–20Ni–20Zr (wt. %) filler metal. Int J Refract Met Hard Mater (2006); 24:247–52.

17. Doherty KJ, Tice JR, Szewczyk ST, Gilde GA. Titanium brazing for structures and survivability. Proceedings of the 3rdInternational Brazing and Soldering Conference; (2006). P. 268–73. San Antonio, Texas, USA.

18. N.K. Mukhopadhyay, P. Paufler, Micro- and nanoindentation techniques for a Mechanical characterization of materials, Int. Mater. Rev. 51 (2006) 209-245.

19. C.A. Schuh, T.G. Nieh, A survey of instrumented indentation studies on metallic glasses, J. Mater. Res. 19 (2004) 46–57.

20. W.C. Oliver, G.M. Pharr, Measurement of Hardness and Elastic Modulus by Instrumented Indentation: Advances in Understanding and Refinements to Methodology, J. Mater. Res. 19 (2004) 3-20.

21. Shiue RK, Wu SK, Chan CH. The interfacial reactions of infrared brazing Cu and Ti with two silver-based braze alloys.J Alloys Compd, 372, (2004); 148–57.

22. M. Calin, J. Eckert, L. Schultz, Improved mechanical behavior of Cu–Ti-based bulk metallic glass by in situ formation of nanoscale precipitates, Scr. Mater. 48 (2003) 653–658.

23. X.H. Lin, W.L. Johnson, Formation of Ti–Zr–Cu–Ni bulk metallic glasses, J. Appl. Phys. 78 (1995) 6514–6519.

 doi:10.20944/preprints201806.0309.v1

24. H. Choi-Yim, R. Busch, W.L. Johnson, The effect of silicon on the glass forming ability of the Cu47Ti34Zr11Ni8 bulk metallic glass forming alloy during processing of composites, J. Appl. Phys. 83 (1998) 7993–7997.
25. M J Donachie. Titanium: a technical guide. 2 ed. USA: ASM; (2000).
26. Chang E, Chen CH. Low-melting-point titanium-base brazing alloys—part 2: characteristics of brazing Ti.21Ni–14Cu on Ti–6Al–4V substrate. JMEPEG (1997); 6:797–803.
27. Metals hand book, vol 3: alloy phase diagrams. ASM; (1992).
28. Schwartz MM. Brazing. 2 ed. USA: ASM; (2003).
29. Dieter GE. Mechanical metallurgy. 3 ed. USA: McGraw Hill; (2001).
30. Oliver W. C. and Pharr G. M., J. Mater. Res. 7 (1992) 1564.
31. JIS Z 3192. Methods for tension and shear tests for brazed joint; 1988.
32. Journal of Phase Equilibria and Diffusion, 35 (2014)2
33. Metallurgical and materials transactions A, 44A (2013)9.
34. Materials transactions Vol.49, No.6 (2008) Pp.1488.